An Infrared and X-ray Absorption Study of the Structure and Equilibrium of Chromate, Bichromate, and Dichromate in High-Temperature Aqueous Solutions

Markus M. Hoffmann,[†,‡] John G. Darab,[§] and John L. Fulton*[,†]

Fundamental Sciences Division and Energy Sciences and Technology Division, Pacific Northwest National Laboratory, Richland, Washington 99352

Received: February 7, 2001; In Final Form: May 10, 2001

The structure and speciation of bichromate, dichromate, and chromate was studied to temperatures up to 400 °C using the combined information obtained from infrared (IR) and X-ray absorption fine structure (XAFS) spectroscopy. Actual species concentrations were obtained from the IR measurements, which were then used as fixed input parameters for the XAFS analysis. With this procedure a complete description of the molecular structure of each chromate species to high temperatures was obtained. In agreement with previous high temperature studies on the chromate system, the bichromate species was found to become thermodynamically favored at high temperatures under acidic or near-neutral conditions. For example, only the bichromate species was found to be present at 350 °C in a 0.145 m aqueous chromate solution having an initial solution pH of 3.3. Because of this, the bichromate molecular structure could be fully characterized from the measured XAFS data. The first-shell structure around the central chrome atom is extremely similar in the bichromate and dichromate structures with virtually identical Cr−O bond distances for the three terminal oxygen atoms and with only a slightly different Cr−O bond distance for the bridging oxygen. As a result of this structural similarity, the $\nu_{as}(CrO_3)$ asymmetric stretching frequency of the bichromate and dichromate species nearly overlap in the IR, as is evident from the quantitative analysis of this band. Furthermore, the chromate structure in the ion-paired species, $(Na^+)(CrO_4^{2-})$, at high temperature is nearly identical to that in the free chromate ion.

Introduction

X-ray absorption fine structure (XAFS) spectroscopy is a widely used experimental tool to obtain both structural and chemical information about a sample of interest. While chemical information such as the oxidation state is contained in the preedge and X-ray absorption near edge (XANES) region, structural information such as bond distances and coordination numbers can be extracted from the extended X-ray absorption fine structure (EXAFS). Such a wealth of information obtainable from XAFS spectroscopy has recently spurred the application of this technique to the study of aqueous solutions to high temperatures.[1] However, very few of these studies have attempted to probe chemically reacting hydrothermal systems wherein the chemical reaction alters any of the chemical and structural parameters mentioned above. In principle, XAFS spectroscopy is well suited to study in situ chemically reacting systems. In practice, it is sometimes difficult to deconvolute the contributions of a multitude of equilibrium species if their concentrations are not known. In favorable cases, the number and concentrations of present species may be obtained directly by independent spectroscopic measurements, such as IR spectroscopy, and these parameters may then be used to examine the EXAFS for structural changes that are associated with the chemical reaction of interest. Here we develop and apply this approach in a study of aqueous chromate solutions to high temperatures. In a previous study[2] at ambient conditions, we have fully characterized the spectral features observable with XAFS and IR spectroscopy that are associated with the structures of CrO_4^{2-}, $HCrO_4^-$, and $Cr_2O_7^{2-}$ or chromate, bichromate, and dichromate, respectively. These chemical equilibria are described by the well-known relationships:

$$CrO_4^{2-} + H^+ \rightleftharpoons HCrO_4^- \quad (1)$$

$$2CrO_4^{2-} + 2H^+ \rightleftharpoons Cr_2O_7^{2-} + H_2O \quad (2)$$

$$2HCrO_4^- \rightleftharpoons Cr_2O_7^{2-} + H_2O \quad (3)$$

In this previous study[2] we found that the local Cr first-shell structure is nearly identical in the bichromate and dichromate structures, in particular with regard to the similarity of the three equivalent terminal bonds ($Cr-O^t$) of the $-CrO_3$ structural unit. With this finding we could explain the observation that the corresponding asymmetric stretching bands, $\nu_{as}(CrO_3)$, for both species have essentially the same frequency and absorption coefficient. With regard to the remaining $Cr-O^b$ bridging bond in both the bichromate and dichromate structures, the results of the previous room temperature study were not fully conclusive, although slight differences for the $Cr-O^b$ bond distances were indicated. Since previous investigations of the bichromate, dichromate, and chromate system to high temperatures indicated that the bichromate becomes the dominant species at high temperatures,[3−5] in situ, hydrothermal EXAFS studies provide another means to determine the structural parameters of the bichromate species. Such detailed knowledge is desirable for a

* Corresponding author. E-mail: john.fulton@pnl.gov. Fax: 509-376-0418.
† Fundamental Sciences Division.
‡ Present address: State University of New York, College at Brockport, Department of Chemistry, Brockport, NY 14420.
§ Energy Sciences and Technology Division.

10.1021/jp0104740 CCC: $20.00
Published on Web 06/26/2001

number of applications[3] that include the understanding of corrosion phenomena of chromium-containing alloys in high-temperature aqueous systems and the understanding of geochemical processes. Another application pertains to the remediation of radioactive wastes that are currently stored at various Department of Energy (DOE) sites and that await vitrification into stable glass waste forms. Chromium species are present in much of these radioactive wastes and they have been identified as a troublesome component from a vitrification standpoint.[6] Cr(III) species such as Cr_2O_3 may also limit the waste loading by reacting with FeO, Fe_2O_3, NiO, and other oxides to form spinel crystals in the melt, which can cause problems during vitrification.[7] It is for these reasons that hydrothermal methods are considered for oxidizing the relatively insoluble Cr(III) oxyhydroxides that occur in the waste sludges to soluble Cr(VI) species in order to decrease the concentration of chromium in the wastes entering the vitrification plant. Therefore, knowledge of the structure and speciation of the chromate species to high temperatures is imperative for the development of these aqueous separation schemes.

Experimental Section

In situ high-temperature/high-pressure spectroscopic measurements are especially challenging for the study of aqueous solutions because of their highly reactive nature. Particular care was placed in the choice of corrosion resistant materials for the design of the experiments. The high-temperature aqueous solutions were only allowed to be in contact with Pt/Ir alloy and diamond window material in both the IR and the XAFS experiments. A detailed description of how this was accomplished can be found elsewhere.[8,9] The utility of IR spectroscopy for studies of hydrothermal systems has recently been reviewed.[10]

Water is highly absorbing in the mid-IR spectral region. Hence, a very short path length of 25.4 μm was established between the two diamond windows (5 mm diameter × 1 mm thick chemical vapor deposition, CVD, disks) of the cell used for the acquisition of the IR spectra. Furthermore, the IR measurements were carried out using deuterated chemicals (D_2O, DNO_3) to avoid water IR bands that interfere with the spectral region of interest from 700 to 1000 cm^{-1}. This allowed us to also investigate the IR region below 875 cm^{-1}. The IR spectra were acquired on a Bruker IFS66V FT-IR instrument. Oscillatory interference fringes in the data that are due to the short optical path length of 25 μm were removed by subtracting a pure D_2O spectrum. At the highest temperatures, most notably in the pH 3.3 data set, the background removal was not fully complete and this led to some very broad, residual bands in the background, as will be pointed out in the Results and Discussion. For all cases, the Levenberg−Marquardt method[11] was used to deconvolute the various IR vibrational bands by fitting to Gaussian-shaped peaks.

For the XAFS experiments, solutions were prepared from solid $Na_2CrO_4 \cdot 4H_2O$ (99%) and, in certain cases, were acidified using concentrated nitric acid (99.9%). For the IR experiments, solid Na_2CrO_4 was used to prepare the samples. All pH values given in the figures and tables refer to room-temperature measurements, not to the pH at the reported experimental conditions. The pH was measured with a meter using a standard Ag/AgCl electode that was calibrated against a series of known buffer solutions.

The XAFS experiments were conducted on the PNC−CAT beam line (ID-20) of the Advanced Photon Source (APS) at Argonne National Laboratory. Both the undulator and monochromator (Si 111 crystal) were scanned for XAFS spectra acquisition. Appropriate standards were used during all measurements to confirm the energy stability of the monochromator. The XAFS data were acquired at the Cr K-edge in transmission mode using standard ionization detectors.

For X-ray energies near the Cr K-edge (6 keV), X-ray absorption by water and the X-ray windows can be relatively high. Hence, a 2.5 mm path length was selected, and the single-crystal diamond windows were only 250 μm thick. The 2.5 mm path length was optimum at higher temperature conditions where the significantly lower solution densities yielded higher transmissions that accordingly improved the counting statistics due to smaller X-ray absorption losses by the solution water.

Standard algorithms[12,13] were employed for the EXAFS data reduction[14,15] that involve the removal of a background function and subsequent fitting of the thereby obtained EXAFS oscillations, $\chi(k)$. The $\chi(k)$ functions of the aqueous chromate data were fit to the standard EXAFS equation,

$$\chi(k) = \sum_i \frac{F_i(k) S_0^{\,2} N_i}{kR_i^{\,2}} e^{-2k^2(\sigma_i^2)} e^{-2R_i/\lambda(k)} \sin\left(2kR_i + \delta_i(k) - \frac{4}{3}k^3 C_{3,i}\right) \quad (4)$$

where $F_i(k)$, $\delta_i(k)$, and $\lambda(k)$ are the amplitude, phase, and mean-free path factors, respectively, derived from the theoretical standard known as the FEFF code.[16] The mean-square variation of the shell distance R_i of N_i backscattering atoms, is given by the so-called Debye−Waller (DW) factor, σ_i^2. The sum in eq 4 is over all possible single scattering paths and for all the significant multiple scattering paths that are calculated to describe the effective scattering amplitudes and phases. We have previously determined,[2] from ambient aqueous CrO_4^{2-} EXAFS data, the single nonstructural parameter, ΔE_o, the constant core−hole factor, S_0^2, and the anharmonicity of the pair distribution,[17] $C_{3,i}$, to be ΔE_o, $= -7$ eV, $S_0^2 = 0.95$, and $C_{3,i} = -5 \times 10^{-5}$ $Å^{-3}$, respectively. Fourier transformations of the k^2-weighted $\chi(k)$ functions were carried out in the k range of $1.5 < k < 12$ $Å^{-1}$ by employing Hanning windows to obtain the presented radial structure plots, $|\tilde{\chi}(R)|$. Fitting of the EXAFS data was done in R space. To assess the goodness of the fit to the experimental data, a fractional misfit $\mathcal{R}$ was calculated according to

$$\mathcal{R} = \frac{\sum_{i=1} |\tilde{\chi}^{\mathrm{fit}}(R_i) - \tilde{\chi}^{\mathrm{exp}}(R_i)|^2}{\sum_{i=1} |\tilde{\chi}^{\mathrm{exp}}(R_i)|^2} \quad (5)$$

where a smaller $\mathcal{R}$ value implies a better fit to the data.[13,18]

Solution densities at high temperatures were determined from the absorption edge height and knowledge of the solution density at room temperature, as previously described.[19,20] The density of the ambient solution was measured with an oscillating-tube densimeter.

Results and Discussion

IR Spectroscopy. *Infrared Spectra and Cr(VI) Speciation.* On the left-hand side of Figure 1, we show a series of IR spectra that were obtained by heating three aqueous chromate solutions to high temperatures. Each solution has a different initial pH value (as measured at 25 °C) of 3.3, 6.3, and 8.5. The indicated

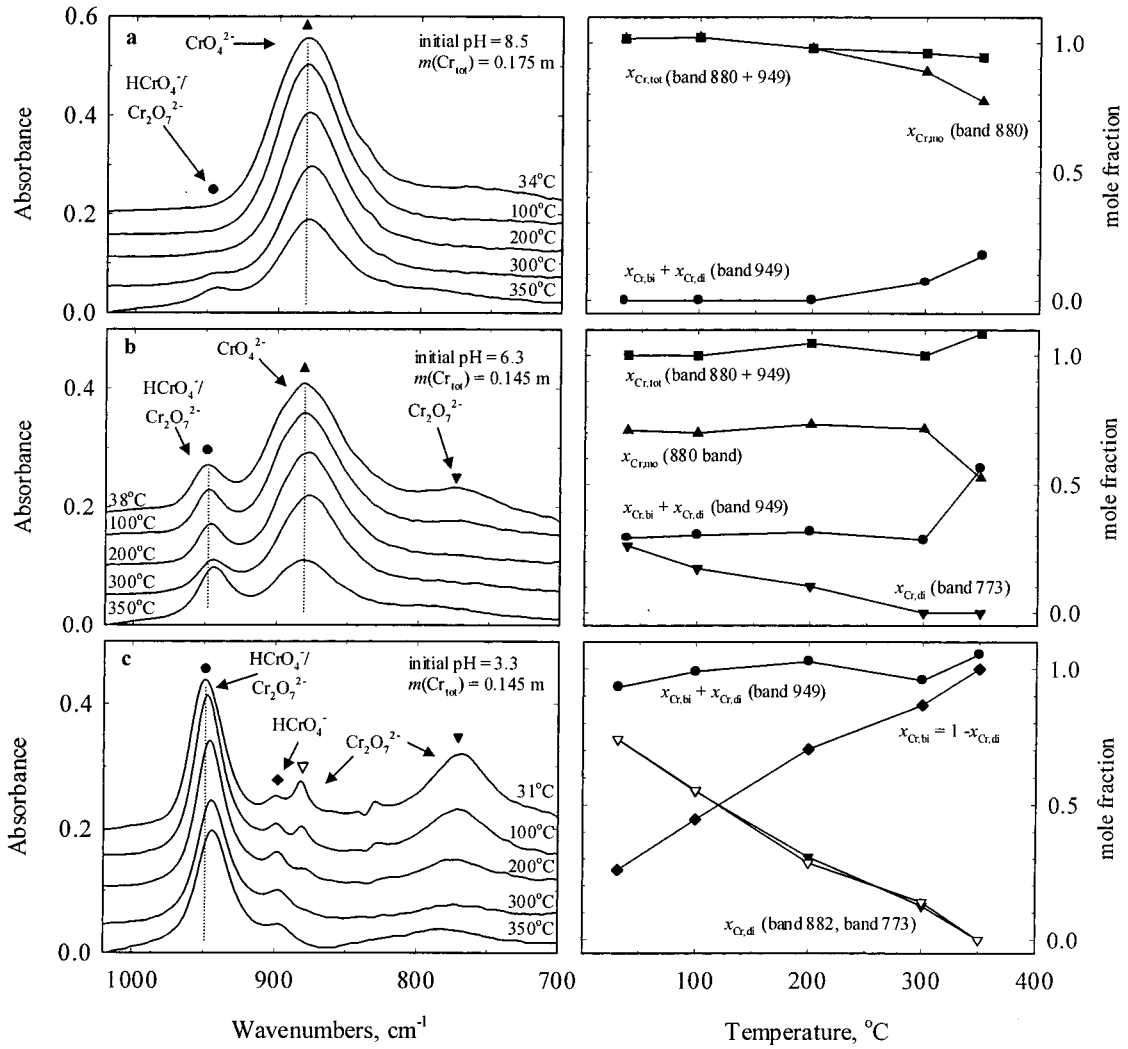

Figure 1. IR spectra obtained from aqueous chromate solutions at a series of high-temperature and high-pressure conditions (left-hand side) having different initial pH values: (a) pH 8.5, (b) pH 6.3, and (c) pH 3.3. For each temperature series, the corresponding pressure conditions were as follows: 34 °C at 273 bar, 100 °C at 273 bar, 200 °C at 273 bar, 300 °C at 342 bar, and 350 °C at 310 bar. The spectra are offset by a constant amount. The plots on the right-hand side give the mole fractions of chrome present as bichromate, $x_{Cr,bi}$, dichromate, $x_{Cr,di}$, and chromate, $x_{Cr,mo}$, that were obtained from the band intensities. The estimated uncertainty for any concentration measurement is about 0.05 mole fraction units.

band assignments for the various vibrational modes of the three equilibrium species CrO_4^{2-}, $HCrO_4^-$, and $Cr_2O_7^{2-}$ were obtained in a previous study under ambient conditions.[2]

One qualitative result is immediately discernible from close inspection of the IR spectra shown on the left-hand side of Figure 1, higher temperatures favor the bichromate species at the studied pH's. In Figure 1a (pH = 8.5), the change in the equilibrium from chromate to bichromate occurs at approximately 300 °C. In Figure 1b (pH = 6.3), more bichromate is formed from both dichromate and chromate at increasing temperatures until all of the dichromate is converted at about 300 °C. Then, at 350 °C additional bichromate is formed from the increasing conversion of chromate. Finally, in Figure 1c (pH = 3.3) the initial dichromate/bichromate mixture at room temperature converts completely into bichromate at 350 °C. These trends were observed to be completely reversible with temperature. These results are more easily depicted by the data plotted in the right-hand side of Figure 1, which shows how the mole fractions $x_{Cr,mo}$, $x_{Cr,bi}$, and $x_{Cr,di}$ vary with temperature. The uncertainties for these measurements are estimated to be about 0.05 mole fraction units. These overall mole fractions refer to the fraction of chrome *atoms* present as CrO_4^{2-} (monomer), $HCrO_4^-$, and $Cr_2O_7^{2-}$, respectively. The choice of "atom-based" mole fractions rather than "species-based" mole fractions simplifies the IR and EXAFS analysis because the total moles of chrome atoms are conserved during the chemical changes but the total moles of the chrome species are not. The species molalities for chromate, bichromate, and dichromate or m_{mo}, m_{bi}, and m_{di}, respectively, are readily obtained from the relationships,

$$m_{mo} = m_{Cr,tot}x_{Cr,mo} \quad m_{bi} = m_{Cr,tot}x_{Cr,bi} \quad m_{di} = m_{Cr,tot}(^1/_2)x_{Cr,di} \tag{6}$$

where $m_{Cr,tot}$ is the total molality of the chrome atoms.

The mole fraction x_i of species i was obtained from its absorption A_i at the peak maximum of the deconvoluted band according to the Beer−Lambert law

$$A_i = \epsilon m_i b = \epsilon_i x_i m_{Cr,tot} \rho b \tag{7}$$

where b is the known fixed path length (25.4 μm) and $m_{Cr,tot}$ is the total system Cr concentration. The solution densities, ρ, were determined from the edge heights of the XAFS spectra. Using this method, the densities of the chromate solutions reported in Table 1 were determined for 200 °C at 273 bar, 300 °C at 342

TABLE 1: Equilibrium Molalities of Chromate Species to High Temperatures[a]

T, °C	ambient	100	200	300	350
P, bar	273	273	273	342	310
ρ, g/cm^{-1}	1.02	1.00	0.88	0.78	0.65
	pH 8.5 Data 0.175 $m_{Cr,tot}$				
m_{mo}	0.178	0.179	0.171	0.155	0.135
m_{bi}	0	0	0	0.013	0.030
	pH 6.3 Data 0.145$m_{Cr,tot}$				
m_{mo}	0.103	0.101	0.106	0.104	0.076
m_{di}	0.019	0.013	0.007		
m_{bi}	0.004	0.019	0.031	0.041	0.081
	pH 3.3 Data 0.145 $m_{Cr,tot}$				
m_{di}	0.054	0.040	0.021	0.010	0.000
m_{bi}	0.038	0.065	0.102	0.126	0.145
log $K_{m,eq3}$	1.58	0.98	0.31		

[a] pH values refer to ambient conditions.

bar, and 400 °C at 411 bar. As expected, these densities were just 5% above the densities of pure water.[21] We previously determined the molal absorption coefficient, ϵ_i, of each band i at ambient conditions.[2] The resulting mole fractions, x_i, reported on the right-hand side of Figure 1 imply that the molal absorption coefficients of these bands are essentially temperature independent since all values for $x_{Cr,tot}$ and ($x_{Cr,bi} + x_{Cr,di}$) from the 949 cm^{-1} band differ from unity by less than 10%. As the only exception, the absorption coefficient of the 900 cm^{-1} band in Figure 1c changes with a temperature increase, mainly because the line shape of this band broadens significantly at temperatures above about 200 °C. For this reason we determine the mole fraction $x_{Cr,bi}$ by subtracting the mole fraction $x_{Cr,di}$ from 1 as shown on the right-hand side of Figure 1c. From the mole fractions and the known total chrome concentration, the species concentrations at each experimental condition were evaluated and listed in Table 1.

It is important to emphasize that the 949 cm^{-1} band represents the mole fraction of the chrome in both bichromate and dichromate. This observation confirms the conclusions from our previous room-temperature chromate study that the 949 cm^{-1} band arises from the $\nu_{as}(CrO_3)$ asymmetric stretching of both the $HCrO_4^-$ and the $Cr_2O_7^{2-}$ molecule.[2] It is also interesting to note that the ligand-to-metal charge-transfer spectra[22] of the bichromate and dichromate are very similar, with major portions of the spectra being identical. This again reinforces the observation that the terminal Cr−O^t bonds are not affected by differences in the bridging oxygens between bichromate (Cr−O−H) and dichromate (Cr−O−Cr). In general, the IR analysis shown in the right-hand side in Figure 1 confirms the applicability of the CrO_4^{2-}, $HCrO_4^-$, and $Cr_2O_7^{2-}$ speciation model of eqs 1−3 for describing the chromate system at higher temperatures.

Equilibrium Constants. A primary purpose of the IR measurements was to obtain the mole fractions shown on the right-hand side of Figure 1, which were then used as fixed input parameters in the EXAFS analysis. It is beyond the scope of this paper to derive from the presented IR data explicit values for the equilibrium constants that could then be directly compared to the values previously reported at much lower concentrations in the studies by Palmer et al.[3] and Chlistunoff and Johnston.[4] Such a comparison would require knowledge of the individual activity coefficients, γ, to obtain the species activities, a. There are no reliable procedures to calculate these activity coefficients for high-temperature conditions in concentrated aqueous solutions (0.145 m). As a further complication in this regard, we also did not independently determine the proton concentrations at high temperatures. However, the observation that the bichromate species is favored at higher temperatures is in agreement with the findings of both Palmer et al.[3] and Chlistunoff and Johnston.[4] In Table 1 we also included values for log$K_{m,eq3}$ for the pH independent reaction of eq 3. These values continually decrease with increasing temperature, as the dichromate species becomes less stable at higher temperatures. Palmer et al.[3] reported log K_{eq1} and log K_{eq2} values for temperatures up to 175 °C at various ionic strengths, from which log K_{eq3} values maybe evaluated according to

$$K_{eq3} = \frac{K_{eq2}}{(K_{eq1})^2} \tag{8}$$

According to their log K_{eq1} and log K_{eq2} values, log K_{eq3} decreases from 1.84 at 25 °C to 1.06 at 175 °C at 0.1 m ionic strength and from 2.00 to 1.18 at 0.5 m ionic strength. The ionic strength of our investigated solution of initial pH 3 was 0.27 at 25 °C decreasing slightly to 0.24 at 200 °C due to the formation of more bichromate from dichromate. Although one cannot directly compare activity-based equilibrium constants with molality-based equilibrium constants, the change of our obtained log $K_{m,eq3}$ from 1.58 at 25 °C to 0.31 at 200 °C is in qualitative agreement with the data of Palmer et al.[3]

(Na^+)(CrO_4^{2-}) Contact-Ion Pair. Generally speaking, there is indeed overwhelming support that ion-pair formation proceeds in aqueous solutions of mono- and bivalent electrolytes at temperatures above approximately 300 °C due to the lower dielectric constant of water.[17,23−25] For aqueous Na_2SO_4 solutions, in which the divalent anion is of similar size to that of chromate, calorimetry measurements[25] show that ion-pair formation would already be well developed at temperatures of about 300 °C for concentrations in this study. In their UV−vis study of the chromate−bichromate equilibrium, Chlistunoff and Johnston[4] observed a pronounced change in the behavior of the spectra at temperatures exceeding 320 °C. The reversing spectral changes as temperature increases from 380 to 400 °C, were ascribed to a shift of the chemical equilibrium to the (K^+)(CrO_4^{2-}) ion-pair species.[4] This observed effect displayed a large density dependence and was much less pronounced at a higher density of 0.533 g/cm^3 than at lower densities. These densities are lower than the densities of the conditions investigated in this study, although our concentration is much higher (0.145 m vs 0.00025 m). From both our IR and XAFS data there is no direct evidence of ion-pair formation, although there are many qualitative indications that such species exist at higher temperatures that we describe below. If the interactions between a sodium ion and a chromate ion were strong enough to form a weak chemical bond to the oxygen atoms (rather than just electrostatic and van der Waals interactions), thereby producing a $NaCrO_4^-$ *molecular* ion similar to that for the proton on bichromate, one would observe new IR bands for this $NaCrO_4^-$ species that would lie close to those for the bichromate ion. This is not observed. Hence, we believe that the Cr−O bonds in the ion-pair species $NaCrO_4^-$, would be nearly identical to those of the free CrO_4^{2-}. The formation of the ion-pair species does not upset the tetrahedral symmetry of chromate, that would result in the appearance of new vibrational modes.

Reinforcing this concept is another qualitative observation. Chlistunoff and Johnston[4] observed that the ligand-to-metal charge transfer (LMCT) bands for the $NaCrO_4^-$ species are nearly identical to those of CrO_4^{2-}. Thus, purely electrostatic (plus van der Waals) interactions of the Na^+ with the O's on the chromate do not upset the nature of the Cr−O bond to the extent that it affects the LMCT bands.

IR Spectral Shifts. The observations about the vibrational spectra for ion-paired tetrahedral chromates is different from that reported for the structurally different, planar NO_3^- ion where significant shifts in the vibrational energies are observed upon formation of the ion-pair species.[26] There are, however, small band shifts that can be seen upon close inspection of the spectra shown on the left-hand side of Figure 1. Small spectral shifts in the range from 1 to 5 cm^{-1} can be observed for the bands located at 800 and 949 cm^{-1}. For the chromate band at 880 cm^{-1} we observed a slight red shift for the 200 °C spectrum and a 2 cm^{-1} shift for the 300 °C. Hence we tentatively assigned this spectral shift to formation of the $(Na^+)(CrO_4^{2-})$ ion pair. As we point out in the later EXAFS analysis, these IR band shifts at approximately 300 °C coincide with a moderate increase in the static disorder of the Cr−O bonds that is also assigned to formation of the ion-pair species. If this interpretation is correct, then the mole fractions of chromate reported in Figure 1 represent the combined mole fractions of CrO_4^{2-} and $(Na^+)(CrO_4^{2-})$. Further, the data in Figure 1a imply that the ion-pair species form first around 200 °C and then, between 300 and 350 °C, small amounts of bichromate are formed.

For the spectra in Figure 1c, the band at 949 cm^{-1} assigned to the bichromate and dichromate species undergoes a 5 cm^{-1} red shift at higher temperatures. Similar to the $CrO_4^{2-}/(Na^+)$-(CrO_4^{2-}) band at 880 cm^{-1}, these changes are most likely due to very slight differences in the vibrational frequency of the terminal Cr−O^t bonds between the dichromate and bichromate species.

Chromic Acid, Dichromic Acid, and Sodium Bichromate. The free chromic acid H_2CrO_4 and/or the free dichromic acid according to

$$CrO_4^{2-} + 2H^+ \leftrightarrows H_2CrO_4 \quad (9)$$

$$Cr_2O_7^{2-} + 2H^+ \leftrightarrows H_2Cr_2O_7 \quad (10)$$

may in principle also be present as equilibrium species at high temperatures. At room temperature, the equilibrium constant for the formation of the chromic acid[27] is not favorable and thus this species exists at only extremely low pH. As we previously discussed,[2] the $\nu_{as}(CrO_2)$ asymmetric stretching band in both of the free acids should be in a similar frequency range as observed for the chromyl halogenides, like CrO_2Cl_2, where this strong band has been found in the vicinity of 1000 cm^{-1}.[28−30] There is no evidence for such a band in the high-temperature IR data on the left-hand side of Figure 1, and the free acids appear to play no important role as equilibrium species at the investigated experimental conditions. Furthermore, the set of ligand-to-metal charge-transfer bands (LMCT) for chromic acid[22] is at significantly different energies than for chromate or bichromate. Again if chromic acid were present, we would expect to see new vibrational bands because of these differences in the energies of the Cr−O molecular orbitals, which we do not observe.

There are three other possible ion-pairing species that could play a role in this system where the Na^+ concentration is relatively high, namely $(Na^+)(HCrO_4^-)$, $(Na^+)(Cr_2O_7^{2-})$, and $(2Na^+)(CrO_4^{2-})$. At temperatures in excess of 350 °C, ionic species tend to form charge-neutral complexes since the dielectric constant of water is so low. In light of the fact that the IR and UV spectral bands of $(Na^+)(CrO_4^{2-})$ are only slightly shifted from those of the free CrO_4^{2-}, it is unlikely that these other ion-pair species would have unique spectral features. A fourth species, $(Na^+)_2(Cr_2O_7^{-2})$ is deemed unlikely since at temperatures where the doubly paired dichromate might exist, the equilibria strongly favor the formation of bichromate species.

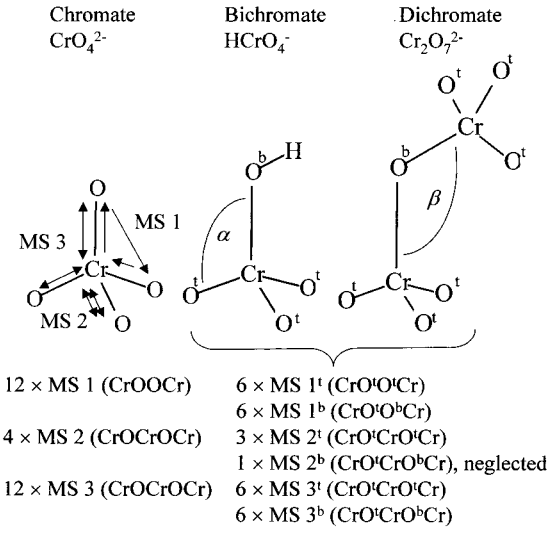

Figure 2. Schematic of the bichromate, dichromate, and chromate structures (reproduced from ref 2). The principal multiple scattering contributions are indicated with their respective degeneracies given below each structure.

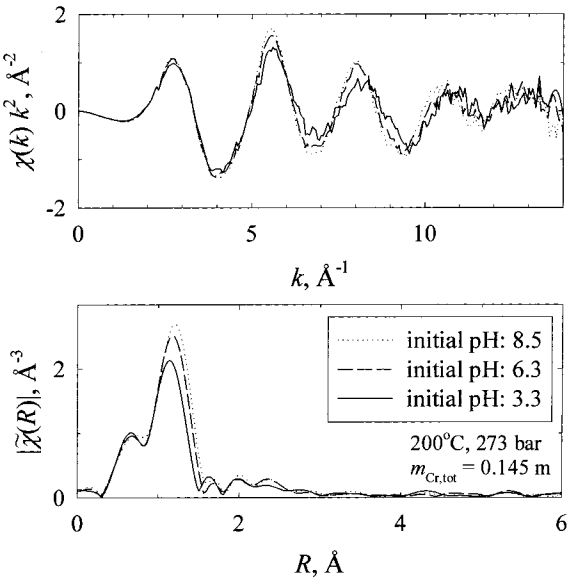

Figure 3. EXAFS spectra of aqueous chromate solutions at 200 °C and 273 bar for initial pH values of 8.5, 6.3, and 3.3. The upper figure gives the $k^2\chi(k)$ functions, whereas the lower figure gives the corresponding radial structure plots obtained from the magnitude of the Fourier transformation of the $\chi(k)$ functions. The different first-shell structures in the chromate, bichromate, and dichromate species give rise to the variations in the spectral features.

EXAFS Spectroscopy. *Spectral Data.* Schematic representations of the structure of the bichromate, dichromate, and chromate ions are given in Figure 2. We previously explained in detail how the structural differences between these ions manifest themselves in the EXAFS spectra under ambient conditions.[2] Similar features are evident in Figure 3, which shows the XAFS spectra at 200 °C and 273 bar for aqueous chromate solutions at three different initial pH values. The nonequivalent chrome−oxygen bond distances (Cr−O^t and Cr−O^b) present in the low-pH, bichromate and dichromate dominant solutions cause the amplitudes of the $\chi(k)$ functions to be smaller than the $\chi(k)$ functions from the chromate dominant solutions at higher solution pH. Accordingly, the intensity of

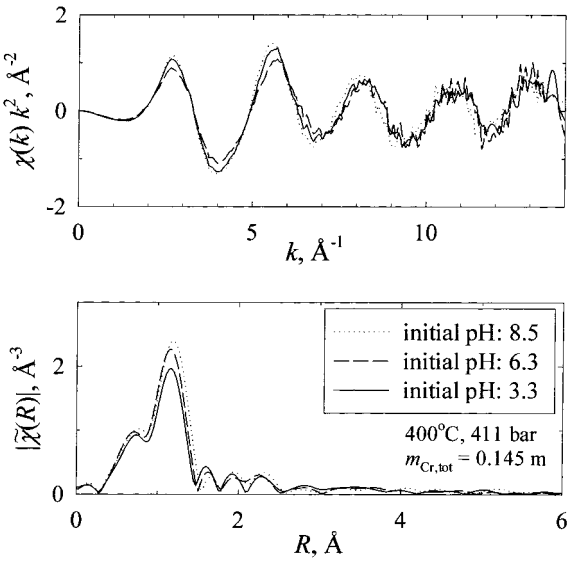

Figure 4. EXAFS spectra of aqueous chromate solutions at 400 °C and 411 bar for initial pH values of 8.5, 6.3, and 3.3. The upper figure gives the $k^2\chi(k)$ functions, whereas the lower figure gives the corresponding radial structure plots obtained from the magnitude of the Fourier transformation of the $\chi(k)$ functions. Spectral differences with corresponding spectra given in Figure 3 are due to changes in the speciation that occur when the temperature is increased to 400 °C.

the main peaks from the Cr−O bonds near 1.2 Å in the radial structure plots in Figure 3 decreases with decreasing solution pH where the bichromate and dichromate species are dominant. Further, since the bond length of the three $Cr-O^t$ bonds in the bichromate and dichromate ions are shorter than the Cr−O bond distance of the chromate ion, the maximum of the main peak shifts to a smaller *R* value in the radial structure plots of Figure 3 with decreasing solution pH. This is also why the phase of the EXAFS oscillations in the $\chi(k)$ data is shifted toward higher *k* values with increasing bichromate and dichromate content. (The shoulder at about 0.8 Å on the left-hand side of the main peaks in the radial structure plots of Figures 3 and 4 is an artifact from incomplete removal of the XAFS background function.)

The IR data of Figure 1 and Table 1 show that the bichromate content increases with increasing temperature for all three pH's. Likewise, similar trends are observed when comparing the 400 °C EXAFS data shown in Figure 4 with the corresponding 200 °C EXAFS plots in Figure 3. Indeed, the amplitudes of the $\chi(k)$ functions of the pH 8.5 and 6.3 data are reduced at 400 °C, and the main peak in the radial structure plot is of lower intensity and slightly shifted to lower *R* values. Hence, the temperature dependence of the EXAFS data from the pH 8.5 and pH 6.3 solutions is in qualitative agreement with the IR data. It is also interesting to observe that the amplitude of the main peak in the radial structure plot for the pH 3.3 data is somewhat lower at 400 °C in Figure 4 than at 200 °C in Figure 3, but the peak position is at a slightly higher *R* value at 400 °C. We will come back to this observation later when discussing the EXAFS analysis of the pH 3.3 data.

EXAFS Spectra and Multiple Equilibria. Generally speaking, the $\chi(k)$ function and radial structure plots for experimental conditions where more than one Cr(VI) species are present (for example, the pH 6.3 data of Figures 3 and 4) can be understood as superpositions of the concentration-weighted contributions from each of the Cr(VI) species. From the IR data presented in the previous section we have determined the mole fractions for each of the corresponding EXAFS conditions, except for the EXAFS data at 400 °C. The speciation for the XAFS data taken at 400 °C was determined in the following way. Of the three different pH's studied, only at pH 3.3 does a single species predominate. Thus, this condition is best suited for structural characterization by EXAFS. For the pH 8.5 data we extrapolated the IR mole fraction $x_{Cr,bi}$ to be approximately 0.25 at 400 °C. For the pH 6.3 data, extrapolation is admittedly difficult, as there are large changes in the species concentrations above 300 °C. We estimated a value of $x_{Cr,bi} = 0.75$ for bichromate species and, accordingly, $x_{Cr,mo} = 0.25$ for the chromate species, since the dichromate concentration is greatly diminished at these conditions.

EXAFS Structural Model. We used the same structural model to fit the EXAFS data as we used previously in a study at ambient conditions.[2] In this scheme, which Pandya originally introduced for the analysis of the CrO_4^{2-} structure at ambient conditions,[31] contributions from multiple scattering (MS) paths are also considered since their contributions are significant at low *k* values in the $\chi(k)$ functions and lead to EXAFS features in the radial structure plots above 2 Å. The principal MS paths and their degeneracies are indicated in Figure 2. The path length of each multiple scattering path is constrained by the chrome−oxygen bond distances and the bond angle α. For the chromate ion, α is the tetrahedral angle of 109.48°. For the bichromate and dichromate ions a value of $\alpha = 106° \pm 8°$ was used. This value was obtained in our previous room temperature study.[2] Fitting of the pH 3.3 temperature series indicated that α does not deviate significantly from this value at high temperatures. As a reasonable approximation, only two Debye−Waller (DW) factors were used for the MS paths, one for all MS 1 paths and another for all MS 2 and MS 3 paths, as indicated in Figure 2.

Fitting parameters for the Cr−Cr single scattering path that is only present in the dichromate ion were included by weighting their contributions with the dichromate mole fractions $x_{Cr,di}$ from the right-hand side of Figure 1. Although the bichromate and the dichromate ion may have slightly different $Cr-O^t$ and $Cr-O^b$ bond distances[2] and DW factors, we used only the fitting parameters $R(Cr-O^t)$, $R(Cr-O^b)$, $\sigma(Cr-O^t)$, and $\sigma(Cr-O^b)$ for characterizing the single scattering paths from these bonds. Hence, these parameters represent average values for the bichromate *and* dichromate ions. In addition, changing experimental conditions from dichromate dominant to bichromate dominant conditions will shift the species-weighting on these fitting parameters and this will reveal trends regarding the structural differences of the bichromate and the dichromate ion, if they exist. In our previous study under ambient conditions (25 °C and 1 bar), this was accomplished by diluting a pH 3.3 chromate solution, thereby changing the bichromate-to-dichromate ratio from 1:4 at high to 1:1 at low total chrome concentration. The results from this study indicated that the Cr first-shell structure must be very similar in the bichromate and dichromate ions with virtually identical $Cr-O^t$ bond distances and, although not fully conclusive, a slightly larger $Cr-O^b$ bond distance for the bichromate ion. The temperature series of the pH 3.3 data shown in Figure 5 allows us to further investigate this matter because at 300 °C about 85% bichromate (with 15% dichromate) is present and at 400 °C only bichromate should be present.

Bichromate Structure at 400 °C. Beginning with the pH 3.3 data, we first discuss the fit results from the EXAFS model that are summarized in Table 2. Table 2 also includes fit results from our previous study at ambient conditions.[2] These structural parameters were derived from fits to the experimental $\chi(k)$ data that are shown as solid lines through the pH 3.3 data in Figure 5.

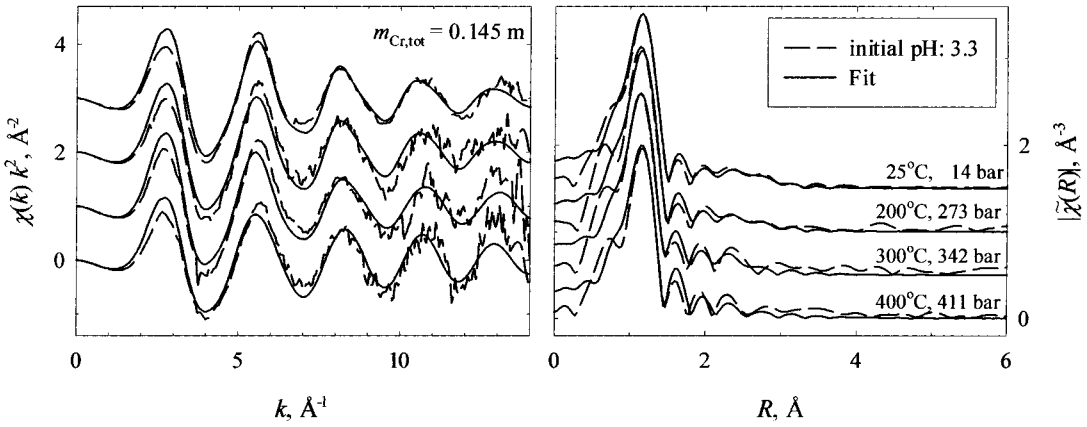

Figure 5. EXAFS spectra of an aqueous chromate solution having an initial pH of 3.3 at the four indicated temperatures and pressures. The left figure gives the $k^2\chi(k)$ functions, whereas the right figure gives the corresponding radial structure plots obtained from the magnitude of the Fourier transformation of the $\chi(k)$ functions. The ambient data are taken from a previous study.[2] Although there is a dramatic increase in the bichromate content at high temperatures, spectral changes are very minor, in particular with regard to the main peak in the radial structure plot that represents the chrome−oxygen single scattering path contributions. Significant spectral changes in the radial structure plots occur between 200 and 300 °C in the region from 2.2 to 2.8 Å, where both the Cr−Cr single scattering path and MS paths contribute.

TABLE 2: EXAFS Analysis of Chromate Species Structures to High Temperatures[a]

T, °C	25[b]	200	300	400
P, bar	14	273	342	411
ρ, g/cm^{-1}	1.02	0.88	0.78	0.56
		pH 3.3 Data		
R(Cr−O^t), (Å)	1.624 ± 0.003	1.625 ± 0.004	1.618 ± 0.004	1.626 ± 0.004
R(Cr−O^b), (Å)	1.824 ± 0.020	1.821 ± 0.030	1.810 ± 0.018	1.872 ± 0.019
R(Cr−Cr), (Å)	3.213 ± 0.025	3.236 ± 0.028	3.249 ± 0.282	
σ^2(Cr−O^t) × 10^{-3}, Å^2	2.61 ± 0.32	2.63 ± 0.46	2.22 ± 0.63	2.09 ± 0.50
σ^2(Cr−O^b) × 10^{-3}, Å^2	10.64 ± 3.63	13.84 ± 6.19	3.31 ± 2.71	3.89 ± 2.73
σ^2(Cr−Cr) × 10^{-3}, Å^2	6.38 ± 2.92	3.15 ± 4.64	9.78 ± 38.13	
σ^2(MS 1) × 10^{-3}, Å^2	5.78 ± 6.04	6.09 ± 6.37	2.13 ± 5.77	6.37 ± 10.52
σ^2(MS 2), σ^2(MS 3) × 10^{-3}, Å^2	33.00 ± 19.80	26.53 ± 17.53	33.10 ± 26.60	26.27 ± 22.58
R[c]	0.014	0.016	0.024	0.031
		pH 8.5 Data		
R(Cr−O), (Å)	1.656 ± 0.003	1.656 ± 0.004	1.657 ± 0.003	1.661 ± 0.004
σ^2(Cr−O) × 10^{-3}, Å^2	1.96 ± 0.34	2.39 ± 0.50	3.31 ± 0.38	3.22 ± 0.53
σ^2(MS 1) × 10^{-3}, Å^2	2.60 ± 5.86	2.95 ± 7.00	0.26 ± 3.69	1.26 ± 5.15
σ^2(MS 2), σ^2 (MS 3) × 10^{-3}, Å^2	37.15 ± 31.53	72.33 ± 114.2	81.06 ± 98.92	75.25 ± 92.87
R[c]	0.035	0.036	0.017	0.023
		pH 6.3 Data[d]		
R[c]		0.025	0.012	0.024

[a] m(Cr$_{tot}$) = 0.145 m; pH refers to ambient conditions. [b] Results were obtained in a previous study at ambient conditions.[2] [c] Fractional misfit as defined in eq 5.[13,18] [d] The model used to fit these spectra is described in the text.

The structural parameters for the pH 3.3 data listed in Table 2 confirm that the first-shell structure around the central chrome atom must be extremely similar for the bichromate and dichromate ion. The Cr−O^t bond distance is virtually unchanged from room-temperature conditions where the bichromate-to-dichromate ratio is 1:4, to 300 °C where the ratio is ∼7:1, and 400 °C where presumably no dichromate remains. This conclusion is in keeping with the observed IR spectra in Figure 1c where the Cr−O asymmetric stretch peak positioned at 949 cm^{-1} moves only a few wavenumbers to lower frequencies with increasing temperatures. Even the Cr−O^b bond distance (Table 2) undergoes perhaps a slight increase at 400 °C. However, the DW factors for the Cr−O^b single scattering path are decreasing with increasing temperature, in particular between 200 and 300 °C. This finding suggests that a decrease in the *static* disorder of the Cr−O^b bond distances occurs as the equilibrium changes from a mixture of bichromate/dichromate at low temperatures to predominantly bichromate at higher temperatures. This implies that the Cr−O^b bond distances are not exactly identical in the bichromate and dichromate. In line with these observations, the EXAFS results in Table 2 indicate that the Cr−O^b bond distance at 400 °C is perhaps 0.06 Å larger than at 300 °C. Furthermore, the analysis of the pH 6.3 data, which we discuss below, also seems to confirm an increased value for the Cr−O^b bond distance at 400 °C for the bichromate.

Between 200 and 300 °C there are significant changes discernible in the radial structure plot between 2.2 and 3.0 Å, where both the MS paths and the Cr−Cr single scattering paths contribute. The Cr−Cr single scattering path distance seems to slightly increase with increasing temperature, although this increase is within the reported uncertainty of the measurements. As a result, the Cr−O^b−Cr bond angle, β, increases slightly but steadily at higher temperatures, from 123.5° at 25 °C to 125.4° at 200 °C and to 127.8° at 300 °C. The uncertainties in the bond distance and DW factor of this path are relatively large for the 300 °C data because at this temperature only less than 15% of all chrome atoms are present as the dichromate species.

There are other possible explanations for these changes that we briefly explored. Chlistunoff and Johnston[4] observed a transition from bichromate to the ion-paired (Na^+)(CrO_4^{2-})

species between 380 and 400 °C, albeit at rather low densities and much higher pH. We explored whether the presence of chromate ions (in the $(Na^+)(CrO_4^{2-})$ ion pair) could account for this observation by adding fixed chromate parameters to the fit. (These parameters were obtained from the pH 8.5 data, which are discussed below.) This change diminished the quality of the fit to the data. We also considered the formation of chromic acid at higher temperatures although there is no specific evidence from the IR data for the presence of the free chromic acid at 350 °C. However, it is possible that this species may be present at the higher temperature of 400 °C because neutral-charged species are strongly favored above 350 °C. This may offer another explanation for the observed larger $Cr-O^b$ bond distance. In the free chromic acid there are two $Cr-O^b$ bonds, which increases the weighting of this bond distance in the EXAFS, leading to a larger average $Cr-O^b$ bond distance. We found that adjusting accordingly the number of $Cr-O^t$ and $Cr-O^b$ single scattering paths would result in a slightly improved fit to the data and would result in values of 1.61 and 1.81 Å for the $Cr-O^t$ and $Cr-O^b$, respectively. It is therefore conceivable that some free chromic acid may be present in experimental conditions of the pH 3.3 data at 400 °C. Finally, the presence of the $(Na^+)(HCrO_4^-)$ ion-pair species is another possibility. However, if this species were present, it would be difficult to distinguish this from the non-Na^+-ion-paired $HCrO_4^-$ in the EXAFS because of the expected high degree of structural similarity.

Chromate Structure at 400 °C. The pH 8.5 data were used to obtain the structural parameters of the chromate ion to high temperatures. In this case, the high-temperature data have the added complication of significant bichromate estimated to be about 25% at 400 °C. Thus, the EXAFS structural parameters derived from the pH 3.3 data at 300 and 400 °C were fixed to account for the relative contributions of bichromate at these temperatures. The Cr−O bond distance of the chromate ion is essentially unchanging, although a very slight increase by 0.003 Å is noted. We also note that above 200 °C, an increasing amount of the chromate will exist in the ion-pair form as $(Na^+)(CrO_4^{2-})$. The DW factor is steadily increasing above 200 °C and the amount of the increase is much larger than can be ascribed to increased thermal disorder. Thus, the formation of the contact-ion pair likely leads to an increase in the static disorder or slight nonequivalency of those Cr−O bonds that are associating with the Na^+. The expected constancy of the Cr−O bond distance to high temperature is similar to the tungstate ion in aqueous solution whose structure has been observed not to change to high temperatures.[9] For this sodium tungstate system, a larger than expected increase in the DW factor may be due to slight W−O bond distortion upon ion-pair formation.

There are several reasons that backscattering for the Cr−Na path for the ion-pair species, $(Na^+)(CrO_4^{2-})$, cannot be directly observed in the EXAFS spectra. Because of the relatively large size of the anion, the electrostatic binding of the cation is relatively weak, as we also deduced from the IR analysis due to the absence of a unique ion-pair peak. The combined effects of the long distances, the relatively high disorder and the less-than-favorable backscattering functions for Na means that the ion-pair species cannot be directly observed. This is in contrast to other systems where the contact-ion-pair species has been fully characterized by EXAFS.[17,32−34]

At room temperature, it is known from neutron scattering experiments[35] that there are 12 water molecules in the first solvation shell around the chromate anion at an average distance of 3.96 Å. This is a relatively large number of water molecules in the first solvation shell, reflecting the large overall size of the chromate anion and further supporting the idea that there is too much disorder in this hydration shell to be observed directly with EXAFS. With increasing temperature, the dielectric constant of the water solvent decreases, reflecting the decreasing hydrogen bonding coordination in water at higher temperatures.[36−41] As a consequence, a reduction in the water coordination number with increasing temperature has been observed for a variety of electrolyte solutions.[17,20,32,42−45] We expect similar dehydration phenomena to occur to a greater extent about molecular chrome species since the binding of water is weaker to these larger polyatomic ions than to small atomic ions.

Finally, the pH 6.3 data essentially serve as confirmation of the fit results obtained from the pH 3.3 and pH 8.5 data. As the fractional misfit, R, indicates, the pH 6.3 data are well reproduced by simply co-adding the fractional contributions from the chromate ion and the bichromate/dichromate ions, using the structural parameters listed in Table 2 for the pH 8.5 and pH 3.3 data.

We then used the pH 6.3 data set to further examine if the $Cr-O^b$ bond distance is changing at higher temperatures. Leaving only the $Cr-O^b$ bond distance as an adjustable fit parameter, we obtained for the pH 6.3 data at 300 °C a value of $R(Cr-O^b) = 1.843 \pm 0.033$ Å and at 400 °C a slightly larger value of $R(Cr-O^b) = 1.857 \pm 0.017$ Å, although the difference is within the reported measurement error. In both cases the fractional misfit R improved slightly by about 0.002 from the R values listed in Table 2 for the pH 6.3 data. Hence, even though the experimental errors are relatively high, these results tend to support a slightly larger $Cr-O^b$ bond distance for the bichromate species that is predominant at higher temperatures.

XANES Spectra. The XANES regions of the chromate, bichromate, and dichromate systems that are shown in the left-hand side of Figure 6 contain several distinct spectral features arising from multielectron transitions that have been studied in detail by Bianconi et al.[46] These multielectron features are more easily revealed in the derivative spectra shown on the right-hand side of Figure 6 where these multielectron features are indicated by asterisks. It is evident from Figure 6 that these multielectron features undergo significant changes both with increasing temperatures and with speciation changes from a chromate-dominant solution to a dichromate/bichromate dominant one. This is especially true for the small ($\underline{1s}$, $\underline{t_2}$, t_2^{*2}) transition near 6000 eV that shows a decline in intensity with increasing temperature and lower pH resulting in a speciation shift from chromate to bichromate/dichromate. As previously mentioned, the pH 8.5 solution at 300−400 °C likely contains the ion-paired $(Na^+)(CrO_4^{2-})$ rather than the free CrO_4^{2-} ion. Hence, because of their highly similar local structure about the Cr, the 6000 eV feature is present for both CrO_4^{2-} and $(Na^+)(CrO_4^{2-})$. The ($\underline{1s}$, $\underline{3p}$, t_2^{*2}) and ($\underline{1s}$, $\underline{3p}$, t_2^1, $\epsilon p1$) transitions near 6045 and 6050 e$\overline{V}$, respectively, appear to be little affected with increasing temperature but are of somewhat lower intensity for the bichromate and dichromate dominant solutions.

Changes in the speciation also affect the single and multiple scattering features of the XANES region between 6010 and 6040 eV. For the 400 °C data, the derivative spectrum of this region becomes flatter as the bichromate content increases from the high-pH derivative spectrum in Figure 6a to the low-pH derivative spectrum in Figure 6c. There are also distinct changes in this region of the high-pH derivative spectra in Figure 6a as a function of temperature. At 200 °C there are two weak maxima in the derivative spectra just visible near 6018 and 6032 eV.

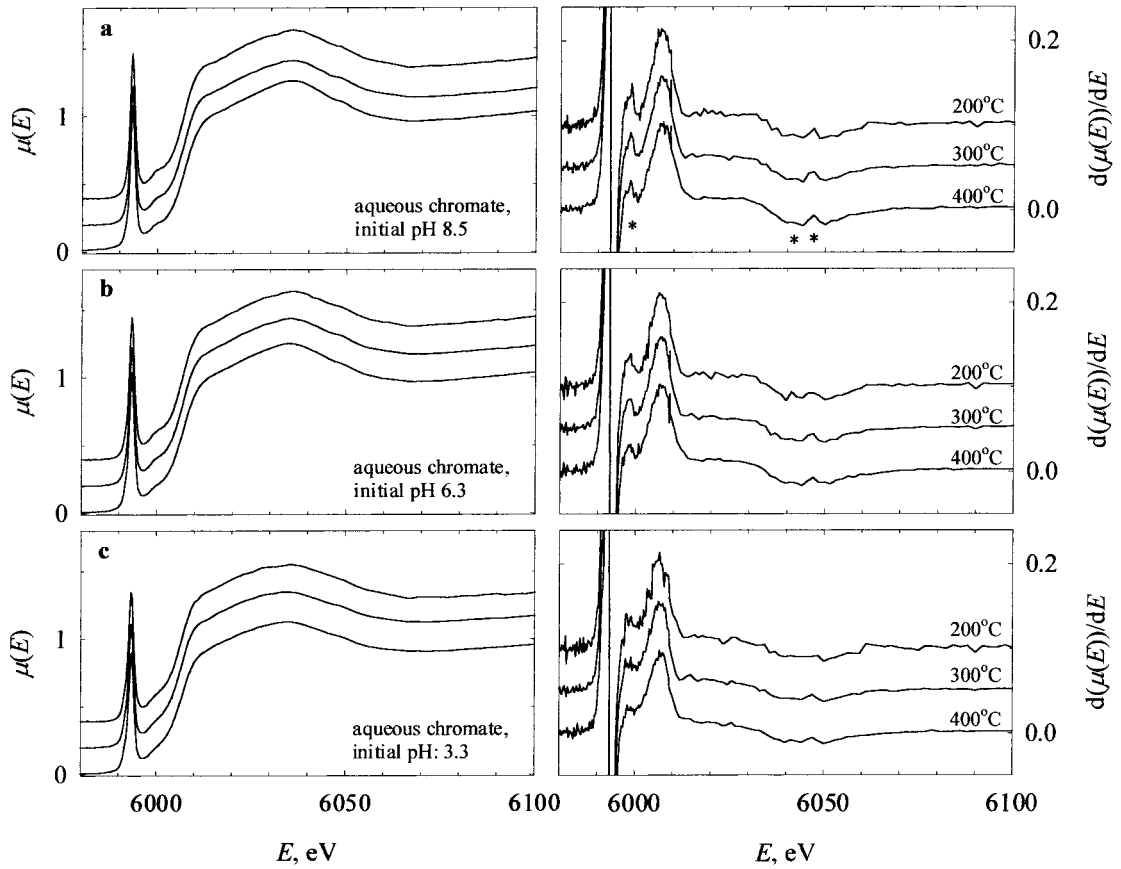

Figure 6. Normalized XANES region (left-hand side) from the *K*-edge of aqueous chromate solutions at a series of high-temperature and high-pressure conditions obtained from aqueous chromate solutions having different initial pH values: (a) pH 8.5, (b) pH 6.3, and (c) pH 3.3. For each temperature series, the corresponding pressure conditions were as follows: 200 °C at 273 bar, 300 °C at 342 bar, and 400 °C at 411 bar. The corresponding derivative plots are shown on the right-hand side. The multielectron transitions are indicated by asterisks. The spectra are offset by a constant amount.

These two features are better defined in the ambient spectra and have been assigned to multiple scattering contributions.[2] These become less pronounced with increasing temperature and eventually merge into one feature at 400 °C. These changes cannot only be due to an increased amount of bichromate present at higher temperatures because these spectral changes become evident at 300 °C, where there is little or no bichromate present. Thus, this is further evidence of the formation of $(Na^+)(CrO_4^{2-})$. The resulting slight bond distortion leads to significant disorder and loss of degeneracy for the multiple scattering paths.

As a final possibility, we note that previous neutron scattering measurements revealed that there are 12 hydration waters at a distance of 3.96 Å around the chromate ion at ambient conditions.[35] Since the distance and the amount of disorder (large DW factors) is relatively large for the hydration shell, any conceivable contributions to the XAFS spectrum would be expected to occur only in the region just above the absorption edge. Hence, it is possible that loss of hydration waters in the first shell at higher temperatures may be an additional contributing factor for the disappearance of the maximum near 6018 eV in the derivative spectra of Figure 6a at high temperatures.

Finally, we would like to point out that in all three data sets of Figure 6, there is no significant change in the intensity of the prominent preedge feature near 5994 eV for any condition of this study. This preedge feature arises from the 1s-to-3d bound state transition that is highly absorbing in chromium(VI)-containing compounds due to the noncentrosymmetric tetrahedral symmetry that allows for considerable mixing of O(2p) and Cr(3d) orbitals. Presence of any Cr(III) species, where this transition is highly forbidden, would notably decrease the intensity of this preedge feature. Therefore, we can be certain that no redox reactions involving any of the chromate species occurred at the investigated temperatures and concentrations.

Conclusions

Structural parameters from reacting hydrothermal systems may be obtained from XAFS spectroscopy when the number and concentrations of present species are available from independent measurements such as IR spectroscopy. With this approach a complete description of the structure of the bichromate, dichromate, and chromate species was obtained in a study of the chemical equilibria of these species to high temperatures, up to 400 °C. The obtained structural results confirm the finding from a previous study at ambient conditions that the first-shell structure around the central chrome atom is extremely similar in the bichromate and dichromate ions.[2] The $Cr-O^t$ bond distances for the three terminal oxygen atoms are virtually identical in the bichromate and the dichromate. The $Cr-O^b$ bond distance for the bridging oxygen is also found to be very similar. The virtually identical $Cr-O^t$ bond distances in the bichromate and dichromate are confirmed by the nearly identical $\nu_{as}(CrO_3)$ asymmetric stretching frequency of the bichromate and dichromate species.

Overall, the chrome−oxygen bond distances in all of the three equilibrium species stay essentially unaltered with increasing temperature. Hence, most of the changes observed in the EXAFS with differing experimental conditions reflect the changes in the species concentrations, which were directly obtained by IR

measurements. Both the IR and XAFS measurements clearly show that the bichromate species becomes thermodynamically favored at high temperatures and that the dichromate species becomes unstable at high temperatures for the investigated pH ranges. These observations are in qualitative agreement with previous studies on the chromate, bichromate, and dichromate equilibria. There is qualitative evidence for the existence of the ion-pair species, $Na^+(CrO_4^{2-})$. Namely, there is a 2 cm^{-1} shift in $\nu_{as}(CrO_3)$ asymmetric stretching frequency as the temperature is increased through the region from 200 to 300 °C and an increase in the disorder of the Cr−O bond as measured by EXAFS.

Acknowledgment. This research was supported by the Director, Office of Environmental Management Sciences, of the U.S. Department of Energy, under contract DE-AC06-76RLO 1830. Work by J.L.F. was supported by the Director, Office of Energy Research, Office of Basic Energy Sciences, Chemical Sciences Division of the U.S. Department of Energy, under contract DE-AC06-76RLO 1830. We thank the beamline personnel for the assistance provided at sector ID-20 of the Advanced Photon Source.

References and Notes

(1) Seward, T. M.; Weslowski, D. J. *Direct Observation and Measurement of Hydrothermal Reactions, Special Issue of Chemical Geology*; Elsevier: New York, 2000; Vol. 167.

(2) Hoffmann, M. M.; Darab, J. G.; Fulton, J. L. *J. Phys. Chem. A* **2001**, *105*, 1772−1782.

(3) Palmer, D. A.; Wesolowski, D.; Mesmer, R. E. *J. Solution Chem.* **1987**, *16*, 443−463.

(4) Chlistunoff, J. B.; Johnston, K. P. *J. Phys. Chem. B* **1998**, *102*, 3993−4003.

(5) Hovey, J. K.; Hepler, L. G. *J. Phys. Chem.* **1990**, *94*, 7821−7834.

(6) Darab, J. G.; Li, H.; Matson, D. W.; Smith, P. A.; MacCrone, R. K. In *Industrial Chemical and Materials Science*; D'Amico, K. L., Terminell, L. J., Shuh, D. K., Eds.; Plenum: New York, 1996; Vol. 167, pp 237−255.

(7) Casler, D. G.; Hrma, P. *Scientific Basis for Nuclear Waste Management XXII*; Wronkiewicz, D. J., Lee, J. H., Eds.; Materials Research Society Symposium Proceedings, V556: Warrendale, PA, 1999; pp 255−262.

(8) Hoffmann, M. M.; Addleman, R. S.; Fulton, J. L. *Rev. Sci. Instrum.* **2000**, *71*, 1552−1556.

(9) Hoffmann, M. M.; Darab, J. G.; Heald, S. M.; Yonker, C. R.; Fulton, J. L. *Chem. Geol.* **2000**, *167*, 89−103.

(10) Brill, T. B. *J. Phys. Chem. A* **2000**, *104*, 4343−4351.

(11) Marquardt, D. W. *J. Soc. Ind. Appl. Math.* **1963**, *11*, 431−441.

(12) Newville, M.; Livins, P.; Yacoby, Y.; Rehr, J. J.; Stern, E. A. *Phys. Rev. B* **1993**, *47*, 14126−14131.

(13) Newville, M.; Ravel, R.; Haskel, D.; Rehr, J. J.; Stern, E. A.; Yacoby, Y. *Physica B* **1995**, *208 & 209*, 154−156.

(14) Teo, B. K. *EXAFS: Basic Principles and Data Analysis*; Springer-Verlag: New York, 1986.

(15) *X-ray Absorption: Principles, Applications, Techniques of EXAFS, SEXAFS and XANES*; Koningsberger, D. C., Prins, R., Eds.; John Wiley & Sons: New York, 1988.

(16) Zabinsky, S. I.; Rehr, J. J.; Ankudinov, A.; Albers, R. C.; Eller, M. J. *Phys. Rev. B.* **1995**, *52*, 2995−3009.

(17) Hoffmann, M. M.; Darab, J. G.; Palmer, B. J.; Fulton, J. L. *J. Phys. Chem. A* **1999**, *103*, 8471−8482.

(18) Haskel, D.; Stern, E. A.; Dogan, F.; Moodenbaugh, A. R. *Phys. Rev. B* **2000**, *61*, 7055−7076.

(19) Fulton, J. L.; Pfund, D. M.; Ma, Y. *Rev. Sci. Instrum.* **1996**, *67* (CD-ROM Issue), 1−5.

(20) Fulton, J. L.; Pfund, D. M.; Wallen, S. L.; Newville, M.; Stern, E. A.; Ma, Y. *J. Chem. Phys.* **1996**, *105*, 2161−2166.

(21) Sato, H.; Uematsu, M.; Watanabe, K.; Saul, A.; Wagner, W. *J. Phys. Chem. Ref. Data* **1988**, *17*, 1439−1490.

(22) Sasaki, Y. *Acta Chem. Scand.* **1962**, *16*, 719−734.

(23) Chialvo, A. A.; Cummings, P. T.; Simonson, J. M.; Mesmer, R. E. *J. Mol. Liq.* **1997**, *73, 74*, 361−372.

(24) Oelkers, E. H.; Helgeson, H. C. *Science* **1993**, *261*, 888−891.

(25) Oscarson, J. L.; Izatt, R. M.; Brown, P. R.; Pawlak, Z.; Gillespie, S. E.; Christensen, J. J. *J. Solution Chem.* **1988**, *17*, 841.

(26) Brill, T. B.; Spohn, P. D. *J. Phys. Chem.* **1989**, *93*, 6224−6231.

(27) Baes, C. F.; Mesmer, R. E. *The Hydrolysis of Cations*; Krieger Publishing Co.: Malabar, FL, 1976.

(28) Hobbs, W. E. *J. Chem. Phys.* **1958**, *28*, 1220−1222.

(29) Varetti, E. L.; Müller, A. *Spectrochim. Acta* **1978**, *34*, 895−898.

(30) Stammreich, H.; Kawai, K.; Tavares, Y. *Spectrochim. Acta* **1959**, *15*, 438−447.

(31) Pandya, K. I. *Physica B* **1994**, *50*, 15509−15512.

(32) Wallen, S. L.; Palmer, B. J.; Fulton, J. L. *J. Chem. Phys.* **1998**, *108*, 4039−4046.

(33) Fulton, J. L.; Hoffmann, M. M.; Darab, J. G.; Palmer, B. J.; Stern, E. A. *J. Phys. Chem. A* **2000**, *104*, 11651−11663.

(34) Fulton, J. L.; Hoffmann, M. H.; Darab, J. G. *Chem. Phys. Lett.* **2000**, *330*, 300−308.

(35) Caminiti, R.; Cilloco, F.; Felici, R. *Mol. Phys.* **1992**, *76*, 681−691.

(36) Gorbaty, Y. E.; Kalinichev, A. G. *J. Phys. Chem.* **1995**, *99*, 5336−5340.

(37) Kalinichev, A. G.; Bass, J. D. *Chem. Phys. Lett.* **1994**, *231*, 301−307.

(38) Chialvo, A. A.; Cummings, P. T. *J. Chem. Phys.* **1994**, *101*, 4466−4469.

(39) Mizan, T. I.; Savage, P. E.; Ziff, R. M. *J. Phys. Chem.* **1996**, *100*, 403−415.

(40) Franck, E. U.; Roth, K. *Discuss. Faraday Soc.* **1967**, *43*, 108−113.

(41) Hoffmann, M. M.; Conradi, M. S. *J. Am. Chem. Soc.* **1997**, *119*, 3811−3817.

(42) Seward, T. M.; Henderson, C. M. B.; Charnock, J. M.; Dobson, B. R. *Geochim. Cosmochim. Acta* **1996**, *60*, 2273−2282.

(43) Seward, T. M.; Henderson, C. M. B.; Charnock, J. M.; Driesner, T. *Geochim. Cosmochim. Acta* **1999**, *63*, 2409−2418.

(44) Wallen, S. L.; Palmer, B. J.; Pfund, D. M.; Fulton, J. L.; Newville, M.; Ma, Y.; Stern, E. A. *J. Phys. Chem. A* **1997**, *101*, 9632−9640.

(45) Pfund, D. M.; Darab, J. G.; Fulton, J. L.; Ma, Y. *J. Phys. Chem.* **1994**, *98*, 13102−13107.

(46) Bianconi, A.; Garcia, J.; Benfatto, M.; Marcelli, A.; Natoli, C. R.; Ruiz-Lopez, M. F. *Phys. Rev. B* **1991**, *43*, 6885−6892.